Natural products may interfere with SARS-CoV-2 attachment to the host cell

Abdo Elfiky (abdo@sci.cu.edu.eg)
Cairo University https://orcid.org/0000-0003-4600-6240

Research Article

Keywords: COVID-19, HSPA5, GRP78, Peptide-protein docking, Molecular dynamics simulation, Natural compounds

Posted Date: April 14th, 2020

DOI: https://doi.org/10.21203/rs.3.rs-22458/v1

Abstract

Objectives: SARS-CoV-2 has been emerged in December 2019 in China, causing deadly (5% mortality) pandemic pneumonia, termed COVID-19. More than one host-cell receptor is reported to be recognized by the viral spike protein, among them is the cell-surface Heat Shock Protein A5 (HSPA5), also termed GRP78 or BiP. Upon viral infection, HSPA5 is upregulated, then translocating to the cell membrane where it is subjected to be recognized by the SARS-CoV-2 spike. In this study, some natural product compounds are tested against the HSPA5 substrate-binding domain β (SBDβ), which reported to be the recognition site for the SARS-CoV-2 spike.

Methods: Molecular docking and molecular dynamics simulations are used to test some natural compounds binding to HSPA5 SBDβ.

Results: The results show high to a moderate binding affinity for the phytoestrogens (Diadiazin, Genistein, Formontein, and Biochanin A), chlorogenic acid, linolenic acid, palmitic acid, caffeic acid, caffeic acid phenethyl ester, hydroxytyrosol, cis-p-Coumaric acid, cinnamaldehyde, and thymoquinone to the HSPA5 SBDβ. Based on its binding affinities, the natural compounds, and some hormones, may interfere with SARS-CoV-2 attachment to the stressed cells.

Conclusion: These compounds can be successful as anti-COVID-19 agents for people with a high risk of cell stress like elders, cancer patients, and front-line medical staff.

Introduction

The Chinese National Health Commission reports a novel human coronavirus (SARS-CoV-2) in December 2019 [1,2]. It was after that declared as a pandemic two months later by the World Health Organization (WHO) [2-5]. Pneumonia associated with SARS-CoV-2, termed COVID-19, is suspected to be due to the first animal to human transmission in a seafood market in Wuhan city in November 2019 [1,6,7]. On 20 January 2020, Chinese authorities confirmed the human-to-human route for virus transmission [1,7]. Today, more than 103,000 reported deaths, from the 1.7 million confirmed infections worldwide, are mainly due to lung failure as a result of SARS-CoV-2 disease. The viral protein responsible for host-cell recognition is the spike protein (1300 amino acids), found in homotrimeric state over the virion particle and characterize coronaviruses. Different host cell receptors are recognized by different coronaviruses such as Heparan Sulfate Proteoglycans, Angiotensin-Converting Enzyme 2 (ACE2), Aminopeptidase N, Heat Shock Protein A5 (HSPA5), furin, and O-Acetylated Sialic Acid [8-12].

HSP5A is the master of the unfolded protein response (UPR) in the lumen of the endoplasmic reticulum (ER) [13]. HSPA5 is responsible for protein homeostasis in the lumen of the ER. Upon cell stress, such as under the condition of viral infection or in the case of cancer cells, HSPA5 is upregulated and translocated to the cytoplasm and cell membrane complexing with other proteins [14-18]. HSPA5 is reported to be cell-

surface exposed and responsible for pathogen entry (such as the fungus Rhizopus *oryzae* and many viruses like Human Papillomavirus, Ebola virus, Zika virus, and human coronaviruses) [8,13,15,19-21].

Different natural products have plenty of active molecules that can block the recognition site of the cell-surface HSPA5 and compete for the viral spike recognition.

The four phytoestrogens daidzein, genistein, formononetin and biochanin A are found in Cicer *arietinum* and proved its estrogenic activity for binding human and murine estrogen receptors alpha and beta *in silico* and it's *in vivo* restoration of the bone thickness for ovariectomized mice in a previous study [22].

It was reported that both palmitic and linoleic acids alone (250μM) induce ER stress in H4IIE liver cells, while the co-treatment of the hepatic cells with palmitic acid (250μM) and linoleic acid (125μM) abolished apoptosis [23]. Linoleic acid (125 μM), but not palmitic acid (250μM), is responsible for cytochrome C release from the mitochondria to the cytoplasm during apoptosis [23]. Additionally, the lipotoxicity of saturated fatty acids like palmitic acid is reversed by the treatment of unsaturated fatty acids, such as α-Linolenic acid in the renal proximal tubular cell line, NRK-52E and chlorogenic acid in rat hepatocytes [24,25].

The pre-treatment of hydroxytyrosol, the bioactive component of olive leaf extract, was successful in ameliorating myocardial infarction-mediated apoptosis, which was induced by the administration of isoproterenol to H9c2 cells [26].

Grape skin polyphenols, including caffeic acid and p-Coumaric acid, protect retinal pigment epithelial cells from photooxidative damage in a previous study [27]. The administration of grape skin extract before exposing the ARPE-19 cells to blue light was successful in reducing apoptosis in a dose-dependent manner. At the same time, GRP78 knockdown inhibited this protective role of the extract [27]. The honeybee hive propolis bioactive component, caffeic acid phenethyl ester (CAPE), induce oxidized protein-mediated ER stress in an autophagy-dependent manner [28]. CAPE treated human SH-SY5Y neuroblastoma cells overexpress ER stress-related genes like HSPA5 and enhance the expression of the autophagy marker, LC3-II (Microtubule-associated protein 1A/1B-light chain 3- phosphatidylethanolamine conjugate) [28,29].

Cinnamaldehyde (found in cinnamon) reported reducing the ER stress in the rat obesity animal model [30]. The anticancer, oxidative and antioxidative properties of cinnamaldehyde are responsible for its potential to be used against breast cancer, prostate cancer, colon cancer, leukemia, HCC and oral cancers [31].

Thymoquinone (found in Nigella *sativa* seeds) was reported to prevent ER stress and mitochondria-induced apoptosis in rat animal model for ischemia-reperfusion in the liver [32]. It reduced the expression of the ER stress determinants, including HSPA5 in rats, while it improved the mitochondrial function leading to liver cell protection against ischemia-reperfusion associated apoptosis [32]. Thymoquinone was

used in free and encapsulated formulations to prevent de-myelination in different brain compartments of Wistar rats while it acts as an anti-inflammatory and remyelinating agent [33-35].

In this study, we tested the active components found in some natural products, known by its involvement in ER stress, against the host cell chaperone protein, HSPA5. Additionally, some physiological hormones and compounds are also tested against the chaperone protein (estrogens, hydrocortisone, cholesterol, progesterone, and Testosterone) aiming to find possible natural sources that can alleviate the rapid spread of the newly emerged coronavirus (SARS-CoV-2) and reduce its impact on patients who have a higher affinity to be infected such as cancer patients.

Materials And Methods

Structural retrieval

The structures of the natural compounds are retrieved from the PubChem database [36]. The structures of phytoestrogens (daidzein, genistein, formononetin and biochanin A, found in Cicer arietinum), palmitic acid (palm oil), linolenic acid (an essential omega-3 fatty acid found in vegetable oils like canola, soybean, flaxseed/linseed, and olive and some nuts), Chlorogenic acid (found in coffee) hydroxytyrosol (found in extra virgin olive oil), caffeic acid (found in many sources including berries, herbs, mushrooms, and coffee beans), caffeic acid phenethyl ester (CAPE, the bioactive component of honeybee hive propolis), p-Coumaric acid (found in fungi, peanuts, tomatoes, and garlic), cinnamaldehyde (found in Cinnamomum verum), and thymoquinone (found in the seeds of Nigella sativa), are retrieved using the following PubChem CIDs; 5281708, 5280961, 5280378, 5280373, 985, 5280934, 1794427, 82755, 689043, 5281787, 1549106, 637511, 10281, respectively. Additionally, the structures of physiological compounds like estrogens (estriol (5756), and β-estradiol (5757)), hydrocortisone (5754), cholesterol (5997), Progesterone (5994), and Testosterone (6013) are retrieved from PubChem database to be tested against HSPA5 SBDβ and compared to the natural compounds.

The only available solved structure in the Protein Data Bank (PDB) for the wild-type and full-length HSPA5 in the open configuration is 5E84 [37,38]. The coordinates of HSPA5 were downloaded and prepared for the docking study (water molecules and ligands are removed while missing Hydrogen atoms are added). National Center for Biotechnology Information (NCBI) nucleotide database was used to retrieve the gene (NC_045512.2) from which spike protein was translated (Expassy translate tool). A model was built with the aid of Swiss Model portal, where SARS HCoV (PDB ID: 6NUR, chain A) was used as a template in a previous study by the author [8,39,40]. Structure analysis and verification server (SAVES) of UCLA was used to validate the model [41]. The validated model of the SARS-CoV-2 spike was energy-optimized using the computational chemistry workspace SCIGRESS in order for the spike structure to be ready for the molecular docking experiments. The minimization of the model was performed using classical mechanics (MM3 force field) after Hydrogen atoms addition [42].

Molecular Docking

Docking experiments (AutoDock Vina software) are performed using the HSPA5 solved structure (PDB ID: 5E84) after 50 ns of classical molecular dynamics simulation (performed using NAMD software) [43-45]. Four different conformations of HSPA5 representing the main four clusters (Chimera software) are used to test the ligands binding [46].

Thirteen different natural products-derived compounds are tested against the four different conformations of the host cell chaperone HSPA5 SBDβ, including; daidzein, genistein, formononetin, biochanin A, palmitic acid, linolenic acid, chlorogenic acid, hydroxytyrosol, caffeic acid, caffeic acid phenethyl ester, p-Coumaric acid, cinnamaldehyde, and thymoquinone. Additionally, six different physiological compounds are also docked to the HSPA5 SBDβ for comparison, including; estriol, estradiol, hydrocortisone, cholesterol, progesterone, and testosterone. All the dockings are done using flexible ligand into flexible active site protocol, where both the ligands and the active site residues (I426, T428, V429, V432, T434, F451, S452, V457, and I459) are treated as flexible during the search for a possible docking conformation using the vina scoring function of AutoDock Vina software [37,43]. The grid boxes for the docking experiments were chosen to be of size 48 × 46 × 56 Å centered at (42.3, 54.9, -29.2) Å (with little differences between the different conformations of the HSPA5).

HADDOCK 2.4 web server is utilized to dock the spike model for SARS-CoV-2 against HSPA5 and the complex of HSPA5 with its docked ligands [47]. The HADDOCK 2.4 easy interface was utilized in the study since there are no restraints to be defined [48]. Again the HSPA5 active site (I426, T428, V429, V432, T434, F451, S452, V457, and I459) is treated as flexible. In contrast, the C480-C488 region of the SARS-CoV-2 spike is treated as the active residues (binding site) in HADDOCK 2.4, as reported in a previous study by the author [8].

After docking, the complexes are examined using the Protein-Ligand Interaction Profiler (PLIP) web server (Technical University of Dresden) [49].

Results And Discussion

Figure 1 shows the 2D structures of the natural product compounds (A) and physiological compounds (B) tested for its binding affinity to cell-surface chaperone HSPA5. The structure of HSPA5 (PDB ID: 5E84) is subjected to 50 ns of molecular dynamics simulation (MDS) to equilibrize its atoms in the presence of 0.154 M NaCl solution (TIP3P water model) at 310^0 K using the CHARMM 36 force field [44,50-52]. Figure 2 A shows the Root Mean Square Deviation (RMSD in Å) (blue line), Radius of Gyration (RoG in Å) (orange line), and the Surface Accessible Surface Area (SASA in $Å^2$) (gray line) for HSPA5 during the 50 ns of MDS. The system is equilibrated starting from about 15 ns, where the RMSD is fluctuating around 5Å, RoG is fluctuates around 30 Å, while SASA values are increasing slowly until 30 ns where the SASA values equilibrated at about 32000 $Å^2$. The per residue Root Mean Square Fluctuations (RMSF) in Å

(figure 2 B) show regular fluctuation pattern except for the region S540-D583 (orange cartoon). The N (blue balls) and C (red balls) termini of the HSPA5 are highly movable (RMSF up to 7.5 Å) as any other free terminals during the MDS. At the same time, the buried region, S540-D583, shows higher fluctuations (RMSF values up to 8.2 Å) in comparison to the other areas of the protein (RMSF values less than 4 Å). The substrate-binding domain α has the most movable part of the protein (S540-D583 region in the orange cartoon), while our target domain, the substrate-binding domain β (cyan cartoon) and nucleotide-binding domain (green cartoon) show fluctuating RMSF 4 Å and down to 1 Å.

Docking results

Figure 3 A shows the average binding affinities of different natural compounds to the HSPA5 SBDβ four different conformations with the error bars representing the standard deviations (SD). Pep42 (red column) is a cyclic peptide that recognizes explicitly cell-surface HSPA5 *in vivo* [13,53]. The average binding affinity of Pep42 is -6.73 ±1.13 kcal/mol, which is used here as a reference to judge other compounds' binding affinities. Phytoestrogens (green columns) show excellent average binding energies to HSPA5 ranging from -6.98 ±0.19 kcal/mol (biochanin A) up to -7.80 ±0.91 kcal/mol (daidzein). Compared to Pep42, the phytoestrogens have at least the same binding affinity to HSPA5 SBDβ. This means that a dietary supplement of phytoestrogens (found in Cicer *arietinum*) may contradict the binding of the SARS-CoV-2 spike to the cell-exposed HSPA5 preventing its recognition by the virus.

For the saturated (palmitic) and unsaturated fatty acids (linoleic and chlorogenic acids) (yellow columns) the same conclusion can be drawn, with a better average binding affinity to HSPA5 for chlorogenic (-7.10 ±0.96 kcal/mol) acid compared to other fatty acids (-6.05 ±0.51 and -5.50 ±0.46 kcal/mol for linoleic and chlorogenic acid, respectively). This pattern of HSPA5 binding affinities is in good agreement with the previous reports of the antagonistic effect of unsaturated fatty acids, chlorogenic and linoleic acids, against the saturated, palmitic, fatty acid which induces ER stress [23-25]. Palmitic, linoleic, and chlorogenic acids may be used to counteract the SARS-CoV-2 recognition of the host cell-surface HSPA5 and hence may reduce the viral attachment. Additionally, the saturated fatty acid, palmitic acid, may be used to target stressed HSPA5-exposed cells (viral infected or cancer cell) and induce ER stress leading to cell apoptosis.

The bioactive component of olive leaf extract, hydroxytyrosol, (bink column) shows moderate average binding affinity (-5.20 ±0.35 kcal/mol) to HSPA5 SBDβ. Hydroxytyrosol succeeded in a previous study as a prophylactic agent against myocardial infarction-mediated apoptosis [26]. For the caffeic and p-Coumaric acids (light blue columns), that are found in grape skin, the average binding affinities to HSPA5 SBDβ are -6.3 ±0.60 and -5.63 ±0.57 kcal/mol, respectively. These values are slightly less than Pep42 (-6.73 ±1.13 kcal/mol), but the differences are not significant. Caffeic and p-Coumaric acids may bind to cell-surface HSPA5 competing for its recognition by viral spike protein and contradict the attachment. The same effect can be concluded from the caffeic acid phenethyl ester (CAPE) (dark blue column) that can be found in honeybee hive propolis (average binding affinity to HSPA5 SBDβ is -7.13 ±0.95 kcal/mol).

This average binding energy value is better than the highly selective cyclic peptide, Pep42, which indicates the potential of CAPE as an HSPA5 SBDβ binder. Additionally, CAPE was reported to induce ER stress in an autophagy-dependent manner in human SH-SY5Y neuroblastoma [28,29]. Cinnamaldehyde (cyan column) and thymoquinone (violet column) show -6.25 ±1.10 and -5.520 ±0.12 kcal/mol average binding energies to HSPA5 SBDβ. These binding energies are comparable to the Pep42 cyclic peptide (-6.73 ±1.13 kcal/mol) and hence the active components of cinnamon and the seeds of Nigella *sativa* may tightly bind to cell-surface HSPA5 and could be successful in contradicting SARS-CoV-2 spike recognition and attachment.

Not only the natural compounds can bind HSPA5 SBDβ with high affinity, but also other physiological molecules. Figure 3 B shows the average binding affinities for the binding of estrogens (estriol and estradiol), cholesterol, progesterone, testosterone, and hydrocortisone (cortisol) to HSPA5 SBDβ. As implicated from the binding energy values, all the physiological compounds can tightly bond the HSPA5 SBDβ with values ranges from -7.20 ±0.58 kcal/mol (Hydrocortisone) up to -8.40 ±0.98 kcal/mol (estradiol). These values are lower (better) than that of the Pep42 cyclic peptide, which reported to target cell-surface HSPA5 (GRP78) *in vivo* selectively. It is important here to point out that HSPA5 SBDβ may act as a receptor for such hormones. The binding energies indicate that cell-surface HSPA5 may be critical for these hormones recognition and hence internalization which not only may downregulate the concentration of cell-surface HSPA5, and its associated chemotherapeutic resistance, but also may play an essential role in hormone internalization for cell-signaling [54,55]. As a consequence, these hormones may also be used as protective molecules during chemotherapy to revert the chemoresistance of the HSPA5 presenting cancer cells.

Tables 1 and 2 summarize the interactions established between the small molecules and the HSPA5. Two types of interactions are dominant, the H-bonding and the hydrophobic interactions. Additionally, π-stacking (residues in bold in the tables) is reported between the residue F451 and the estrogens (estriol and estradiol), phytoestrogens (daidzein, genistein, and formononetin), caffeic acid phenethyl ester (CAPE), and cis-p-Coumaric acid. Also, salt bridges (underlined residues in table 1) are formed between the residue K460 and both linolenic acid and cis-p-Coumaric acid. Hydrophobic interactions are more dominant compared to the H-bonding, as can be seen from almost all the natural and physiological compounds. This is in good agreement with previous reports defining the function of HSPA5 SBDβ in the lumen of ER as to recognize unfolded proteins in the lumen of the ER mediating its degradation or refolding using cellular machinery [13,56,57]. On the other hand, hydrocortisone and chlorogenic acid have more H-bonds than hydrophobic interactions (5:3 and 7:5 for hydrocortisone and chlorogenic acid, respectively). Additionally, caffeic acid forms four H-bonds and four hydrophobic contacts with the HSPA5 SDBβ.

Table 1: *The interactions formed between some natural product bioactive compounds and HSPA5 SBDβ upon docking. One docking trial is selected here to represent one conformation of the HSPA5 during 50 ns MDS. Bold residues are interacting through π-Stacking, while underlined residues are forming salt bridges.*

Compound	*AutoDock score (kcal/mol)*	*H-bonding*		*Hydrophobic interaction*	
		number	Amino acids involved	number	Amino acids involved
Daidzein	-8.6	0	N/A	8	Q449, F451, **F451**, I459(3), K460, V495
Genistein	-7.5	1	T458	10	I426(2), T428, T434, Q449, F451, **F451**, V453, V457, I459
Formononetin	-7.5	2	T458(2)	11	I426(2), T428, T434, F451(2), **F451**, V453(2), V457, I459
Biochanin A	-6.9	5	E427(2), K460(3)	8	E427, V429, F451, V453(3), I459, K460
Chlorogenic acid	-6.8	7	E427, V429, S452(3), T458(2)	5	T428, V429, F451(2), V453
Linolenic acid	-6.5	3	T458, K460, K460	16	I426, T428(3), V429(2), Q449(2), F451(4), I459(2), V495, F497
Palmitic acid	-5.5	2	Q449, I450	13	E427, V429, Q449, F451(4), V453, T458, I459(3), F497
Caffeic acid	-6.2	4	F451, V453, I483(2)	4	L480, I483(2), I493
Caffeic acid phenethyl ester (CAPE)	-6.5	2	S452, T458	7	T428, V429(2), F451, **F451(2)**, V453
Hydroxytyrosol	-5.2	2	E427, K460	5	I426, F451(2), I459(2)
cis-p-Coumaric acid	-5.6	3	E427, T458, K460	5	E427, V429, **F451**, V453, I459

Table 2*: The interactions formed between six physiological compounds and HSPA5 SBDβ upon docking. One docking trial is selected here to represent one conformation of the HSPA5 during 50 ns MDS. Bold residues are interacting through π-Stacking.*

Compound	*AutoDock score (kcal/mol)*	*H-bonding*		*Hydrophobic interaction*	
		number	Amino acids involved	number	Amino acids involved
Estriol	-9.1	2	E427, Q449	11	E427, Q449, F451(3), **F451**, V457, I459(3), K460
Estradiol	-8.3	1	T458	6	T428, V429(2), F451, **F451**, V453
Hydrocortisone (Cortisol)	-7.0	5	E427, T456(3), K460	3	E427, F451, I459
Cholesterol	-7.3	0	N/A	6	T428, V429, Q449, F451(2), T458
Progesterone	-7.6	0	N/A	8	I426, E427, F451(4), I459(2)
Testosterone	-8.9	0	N/A	7	I426, E427, F451(4), V457

Figure 4 shows the interaction analysis made by the PLIP web server for the docked structures of HSPA5 to estrogen (estradiol) (A), phytoestrogens (daidzein) (B), and biochanin A (C) as an example. The HSPA5 is shown in colored surface representations with its domains labeled. The ligands are represented in yellow sticks, where it appears how it fit in the binding site groove of the SBDβ. Enlarged views of the binding sites show how the interactions established upon docking. Residues in the binding site of HSPA5 SBDβ are represented in blue sticks and labeled with its one-letter code. In figure 4, the hydrophobic interactions are described in dashed-gray lines, while H-bonds and π-stacking are depicted in solid blue lines and dashed-green lines, respectively. Docking scores are listed to reflect a binding affinity for each complex. Noticeably, the interacting residues are mainly hydrophobic, while hydrophobic interactions are dominant all the docking complexes. For estradiol, only one H-bond is formed through T458, while none is reported in daidzein. On the other hand, the biochanin A-HSPA5 complex show 5 H-bonds. Estradiol and daidzein but not biochanin A form π-stacking with residue F451 of HSPA5.

We performed molecular docking experiments using the four different conformations of HSPA5 after the 50 ns MDS using HADDOCK 2.4. The docking scores range from -94 to -140, indicating high binding affinity between the interacting proteins. Additionally, we tried to dock the small molecules-HSPA5 complexes to the SARS-CoV-2 spike protein model, but the spike doesn't fit the HSPA5 binding site; this may be due to the presence of the small molecules in the SBDβ of HSPA5. The small molecules prevent the spike from binding to HSPA5 SBDβ *in silico*. Our results support the effectiveness of natural products and physiological hormones to block HSPA5 SDBβ, preventing SARS-CoV-2 spike recognition. The small molecules tested in this study may be used as prophylactic agents for high-risk personals like elders, medical staff in the front-line, or cancer patients.

Conclusion

The newly emerged human coronavirus pandemic is the health crisis we encounter in the 21 century, leaving more than 100000 deaths and 1.6 million reported cases. Natural products are known historically for its pharmaceutical properties. In this study, we tried to illuminate the route that some natural product active compounds may utilize though the human cell-surface receptor HSPA5 and its impact on SARS-CoV-2 attachment. These natural compounds or hormones may be used to reduce the risk of COVID-19 for high-risk people like elders and cancer patients or the front-line medical staff.

Declarations

Competing Interest

The author declares that there is no competing interest in this work.

Data Availability

The docking structures are available upon request from the corresponding author

Acknowledgment

The author is thankful to Prof. Dr. Wael Elshemey for the valuable discussions and for performing the optimization of the spike model on his computational facility. MDS calculations are conducted on the supercomputing facility of the Biblioteca Alexandrina, Alexandria, Egypt.

References

1. Hui DS, I Azhar E, Madani TA, et al. The continuing 2019-nCoV epidemic threat of novel coronaviruses to global health — The latest 2019 novel coronavirus outbreak in Wuhan, China. *International Journal of Infectious Diseases.* 2020;91:264-266.
2. Bogoch II, Watts A, Thomas-Bachli A, Huber C, Kraemer MUG, Khan K. Pneumonia of Unknown Etiology in Wuhan, China: Potential for International Spread Via Commercial Air Travel. *Journal of Travel Medicine.* 2020.
3. Organization WH. *Surveillance case definitions for human infection with novel coronavirus (nCoV): interim guidance v1, January 2020.* World Health Organization;2020.
4. Organization WH. *Laboratory testing of human suspected cases of novel coronavirus (nCoV) infection: interim guidance, 10 January 2020.* World Health Organization;2020.
5. Organization WH. *Infection prevention and control during health care when novel coronavirus (nCoV) infection is suspected: interim guidance, January 2020.* World Health Organization;2020.
6. Parr J. Pneumonia in China: lack of information raises concerns among Hong Kong health workers. British Medical Journal Publishing Group; 2020.
7. Yang L. China confirms human-to-human transmission of coronavirus. 2020.
8. Ibrahim IM, Abdelmalek DH, Elshahat ME, Elfiky AA. COVID-19 spike-host cell receptor GRP78 binding site prediction. *Journal of Infection.* 2020.
9. Huang X, Dong W, Milewska A, et al. Human Coronavirus HKU1 Spike Protein Uses O-Acetylated Sialic Acid as an Attachment Receptor Determinant and Employs Hemagglutinin-Esterase Protein as a Receptor-Destroying Enzyme. *J Virol.* 2015;89(14):7202-7213.
10. Raj VS, Mou H, Smits SL, et al. Dipeptidyl peptidase 4 is a functional receptor for the emerging human coronavirus-EMC. *Nature.* 2013;495(7440):251-254.
11. Belouzard S, Millet JK, Licitra BN, Whittaker GR. Mechanisms of coronavirus cell entry mediated by the viral spike protein. *Viruses.* 2012;4(6):1011-1033.
12. Hofmann H, Pyrc K, van der Hoek L, Geier M, Berkhout B, Pohlmann S. Human coronavirus NL63 employs the severe acute respiratory syndrome coronavirus receptor for cellular entry. *Proc Natl Acad Sci U S A.* 2005;102(22):7988-7993.
13. Ibrahim IM, Abdelmalek DH, Elfiky AA. GRP78: A cell's response to stress. *Life Sciences.* 2019;226:156-163.

14. Al-Hashimi AA, Rak J, Austin RC. Cell Surface GRP78: A Novel Regulator of Tissue Factor Procoagulant Activity. *Cell Surface GRP78, a New Paradigm in Signal Transduction Biology*: Elsevier; 2018:63-85.
15. Pujhari S, Macias VM, Nissly RH, Nomura M, Kuchipudi SV, Rasgon JL. Heat shock protein 70 (Hsp70) is involved in the Zika virus cellular infection process. *bioRxiv.* 2017:135350.
16. Nain M, Mukherjee S, Karmakar SP, et al. GRP78 is an important host-factor for Japanese encephalitis virus entry and replication in mammalian cells. *Journal of virology.* 2017:JVI. 02274-02216.
17. Chen T, Xu S. Chronic Exposure of Cisplatin Induces GRP78 Expression in Ovarian Cancer. Paper presented at: Proceedings of the 2017 4th International Conference on Biomedical and Bioinformatics Engineering2017.
18. Misra UK, Gonzalez-Gronow M, Gawdi G, Pizzo SV. The Role of MTJ-1 in Cell Surface Translocation of GRP78, a Receptor for α₂-Macroglobulin-Dependent Signaling. *The Journal of Immunology.* 2005;174(4):2092-2097.
19. Elfiky AA. The antiviral Sofosbuvir against mucormycosis: an in silico perspective. *Future Virology.* 2019;14(11):739-744.
20. Elfiky AA. Human papillomavirus E6: Host cell receptor, GRP78, binding site prediction. *Journal of Medical Virology.* 2020;n/a(n/a).
21. Elfiky AA. Ebola Virus glycoprotein GP1 – host cell surface HSPA5 binding site prediction. *Cell Stress and Chaperones.* 2020;In press.
22. Sayed AA, Elfiky AA. In silico estrogen-like activity and in vivo osteoclastogenesis inhibitory effect of Cicer arietinum extract. *Cell Mol Biol(Noisy-le-grand).* 2018;64(5):29-39.
23. Zhang Y, Xue R, Zhang Z, Yang X, Shi H. Palmitic and linoleic acids induce ER stress and apoptosis in hepatoma cells. *Lipids in Health and Disease.* 2012;11(1):1.
24. Katsoulieris E, Mabley JG, Samai M, Green IC, Chatterjee PK. α-Linolenic acid protects renal cells against palmitic acid lipotoxicity via inhibition of endoplasmic reticulum stress. *European Journal of Pharmacology.* 2009;623(1):107-112.
25. Zhang Y, Miao L, Zhang H, Wu G, Zhang Z, Lv J. Chlorogenic acid against palmitic acid in endoplasmic reticulum stress-mediated apoptosis resulting in protective effect of primary rat hepatocytes. *Lipids in Health and Disease.* 2018;17(1):270.
26. Wu L-X, Xu Y-Y, Yang Z-J, Feng Q. Hydroxytyrosol and olive leaf extract exert cardioprotective effects by inhibiting GRP78 and CHOP expression. *Journal of biomedical research.* 2018;32(5):371-379.
27. Zhao Z, Sun T, Jiang Y, et al. Photooxidative damage in retinal pigment epithelial cells via GRP78 and the protective role of grape skin polyphenols. *Food and Chemical Toxicology.* 2014;74:216-224.
28. Tomiyama R, Takakura K, Takatou S, et al. 3,4-dihydroxybenzalacetone and caffeic acid phenethyl ester induce preconditioning ER stress and autophagy in SH-SY5Y cells. *Journal of Cellular Physiology.* 2018;233(2):1671-1684.

29. Tanida I, Ueno T, Kominami E. LC3 and Autophagy. *Methods Mol Biol.* 2008;445:77-88.
30. Neto JGO, Boechat SK, Romão JS, Pazos-Moura CC, Oliveira KJ. Treatment with cinnamaldehyde reduces the visceral adiposity and regulates lipid metabolism, autophagy and endoplasmic reticulum stress in the liver of a rat model of early obesity. *The Journal of Nutritional Biochemistry.* 2020;77:108321.
31. Hong S-H, Ismail IA, Kang S-M, Han DC, Kwon B-M. Cinnamaldehydes in Cancer Chemotherapy. *Phytotherapy Research.* 2016;30(5):754-767.
32. Bouhlel A, Ben Mosbah I, Hadj Abdallah N, et al. Thymoquinone prevents endoplasmic reticulum stress and mitochondria-induced apoptosis in a rat model of partial hepatic warm ischemia reperfusion. *Biomedicine & Pharmacotherapy.* 2017;94:964-973.
33. Fahmy HM, Noor NA, Mohammed FF, Elsayed AA, Radwan NM. Nigella sativa as an anti-inflammatory and promising remyelinating agent in the cortex and hippocampus of experimental autoimmune encephalomyelitis-induced rats. *The Journal of Basic & Applied Zoology.* 2014;67(5):182-195.
34. Fahmy HM, Fathy MM, Abd-elbadia RA, Elshemey WM. Targeting of Thymoquinone-loaded mesoporous silica nanoparticles to different brain areas: In vivo study. *Life Sciences.* 2019;222:94-102.
35. Noor NA, Fahmy HM, Mohammed FF, Elsayed AA, Radwan NM. Nigella sativa amliorates inflammation and demyelination in the experimental autoimmune encephalomyelitis-induced Wistar rats. *International journal of clinical and experimental pathology.* 2015;8(6):6269-6286.
36. Kim S, Thiessen PA, Bolton EE, et al. PubChem substance and compound databases. *Nucleic acids research.* 2015;44(D1):D1202-D1213.
37. Yang J, Nune M, Zong Y, Zhou L, Liu Q. Close and Allosteric Opening of the Polypeptide-Binding Site in a Human Hsp70 Chaperone BiP. *Structure.* 2015;23(12):2191-2203.
38. Yang J, Zong Y, Su J, et al. Conformation transitions of the polypeptide-binding pocket support an active substrate release from Hsp70s. *Nature Communications.* 2017;8(1):1201.
39. Biasini M, Bienert S, Waterhouse A, et al. SWISS-MODEL: modelling protein tertiary and quaternary structure using evolutionary information. *Nucleic Acids Research.* 2014;42(W1):W252-W258.
40. NCBI. National Center of Biotechnology Informatics (NCBI) database website http://www.ncbi.nlm.nih.gov/. 2020; http://www.ncbi.nlm.nih.gov/, 2020.
41. SAVES. Structural Analysis and Verification Server website 2020.
42. Lii JH, Allinger NL. Molecular mechanics. The MM3 force field for hydrocarbons. 3. The van der Waals' potentials and crystal data for aliphatic and aromatic hydrocarbons. *Journal of the American Chemical Society.* 1989;111(23):8576-8582.
43. Trott O, Olson AJ. AutoDock Vina: Improving the speed and accuracy of docking with a new scoring function, efficient optimization, and multithreading. *Journal of Computational Chemistry.* 2010;31(2):455-461.

44. Phillips JC, Braun R, Wang W, et al. Scalable molecular dynamics with NAMD. *Journal of Computational Chemistry.* 2005;26(16):1781-1802.
45. Humphrey W, Dalke A, Schulten K. VMD: visual molecular dynamics. *J Mol Graph.* 1996;14(1):33-38, 27-38.
46. Pettersen EF, Goddard TD, Huang CC, et al. UCSF Chimera—a visualization system for exploratory research and analysis. *Journal of computational chemistry.* 2004;25(13):1605-1612.
47. van Dijk AD, Bonvin AM. Solvated docking: introducing water into the modelling of biomolecular complexes. *Bioinformatics.* 2006;22(19):2340-2347.
48. de Vries SJ, van Dijk M, Bonvin AM. The HADDOCK web server for data-driven biomolecular docking. *Nat Protoc.* 2010;5(5):883-897.
49. Salentin S, Schreiber S, Haupt VJ, Adasme MF, Schroeder M. PLIP: fully automated protein–ligand interaction profiler. *Nucleic acids research.* 2015;43(W1):W443-W447.
50. Ibrahim A. Noorbatcha, Khan AM, Salleh HM. Molecular Dynamics Studies of Human ?-Glucuronidase. *American Journal of Applied Sciences.* 2010;7(6):823-828.
51. Mark P, Nilsson L. Structure and dynamics of the TIP3P, SPC, and SPC/E water models at 298 K. *The Journal of Physical Chemistry A.* 2001;105(43):9954-9960.
52. Rappe AK, Casewit CJ, Colwell KS, Goddard WA, Skiff WM. UFF, a full periodic table force field for molecular mechanics and molecular dynamics simulations. *Journal of the American Chemical Society.* 1992;114(25):10024-10035.
53. Kim Y, Lillo AM, Steiniger SC, et al. Targeting heat shock proteins on cancer cells: selection, characterization, and cell-penetrating properties of a peptidic GRP78 ligand. *Biochemistry.* 2006;45(31):9434-9444.
54. Zhang L-Y, Li P-L, Xu A, Zhang X-C. Involvement of GRP78 in the resistance of ovarian carcinoma cells to paclitaxel. *Asian Pac J Cancer Prev.* 2015;16(8):3517-3522.
55. Niu Z, Wang M, Zhou L, Yao L, Liao Q, Zhao Y. Elevated GRP78 expression is associated with poor prognosis in patients with pancreatic cancer. *Scientific reports.* 2015;5:16067.
56. Roller C, Maddalo D. The molecular chaperone GRP78/BiP in the development of chemoresistance: mechanism and possible treatment. *Frontiers in pharmacology.* 2013;4:10.
57. Pfaffenbach KT, Lee AS. The critical role of GRP78 in physiologic and pathologic stress. *Current opinion in cell biology.* 2011;23(2):150-156.

Figures

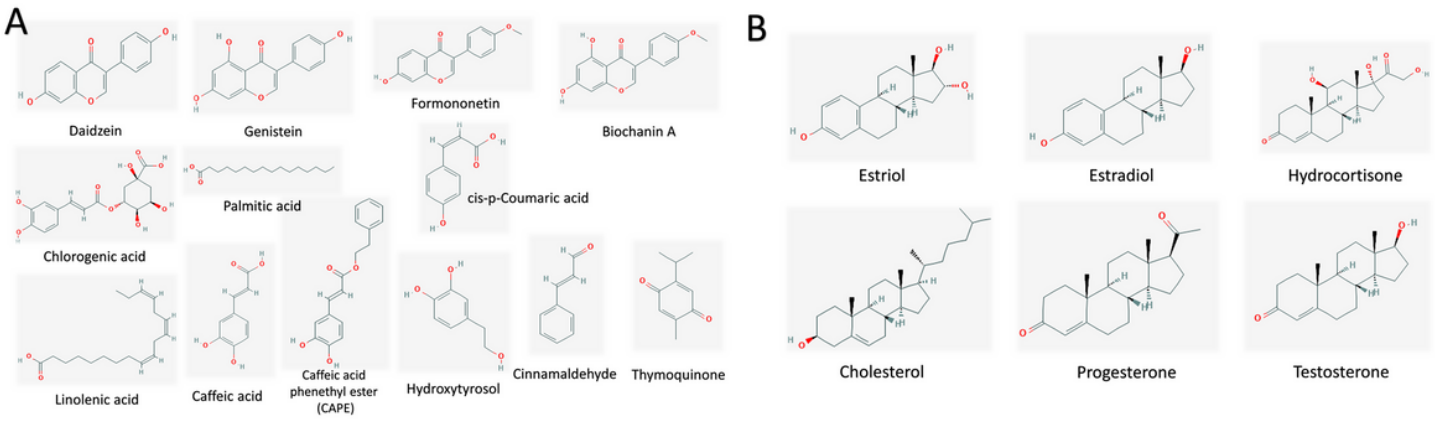

Figure 1

2D structures of the natural product derived compounds (A) and physiological compounds (B).

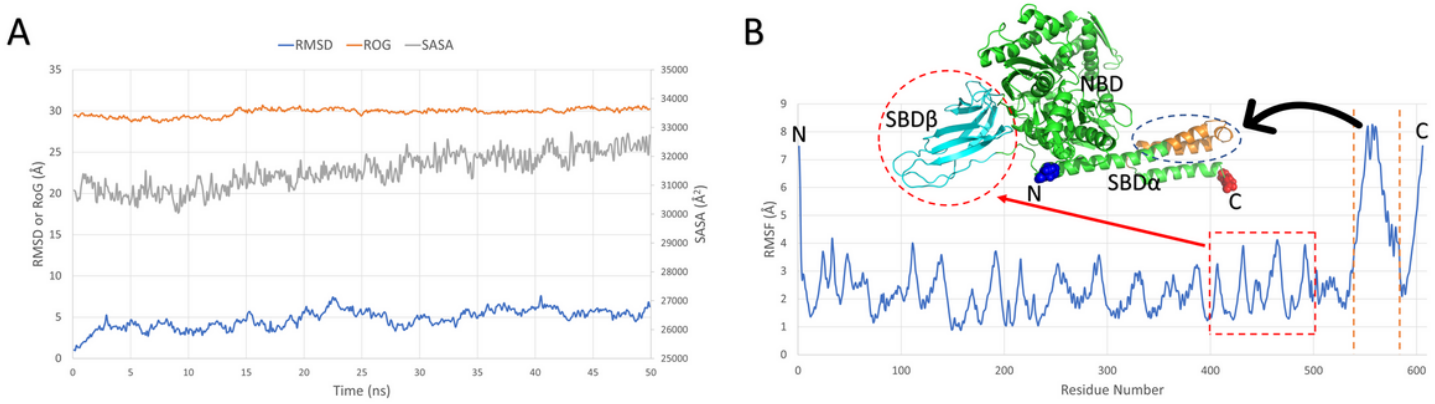

Figure 2

(A) Root Mean Square Deviation (RMSD) in Å (blue line), Radius of Gyration (RoG) in Å (orange line), and Surface Accessible Surface Area (SASA) in Å2 (gray line) versus time in ns for HSPA5. MDS is performed using CHARMM 36 force field by NAMD. (B) per residue, Root Mean Square Fluctuations (RMSF) in Å (blue line). The structure of HSPA5 is shown in the colored carton with its domain labeled NBD (nucleotide-binding domain) SBD (substrate-binding domains). Blue and red balls, respectively represent N and C terminals of the protein. SBDβ is depicted in cyan cartoon and indicated in the RMSF histogram, while the most movable internal region of HSPA5 (S540-D583) is represented in the orange cartoon.

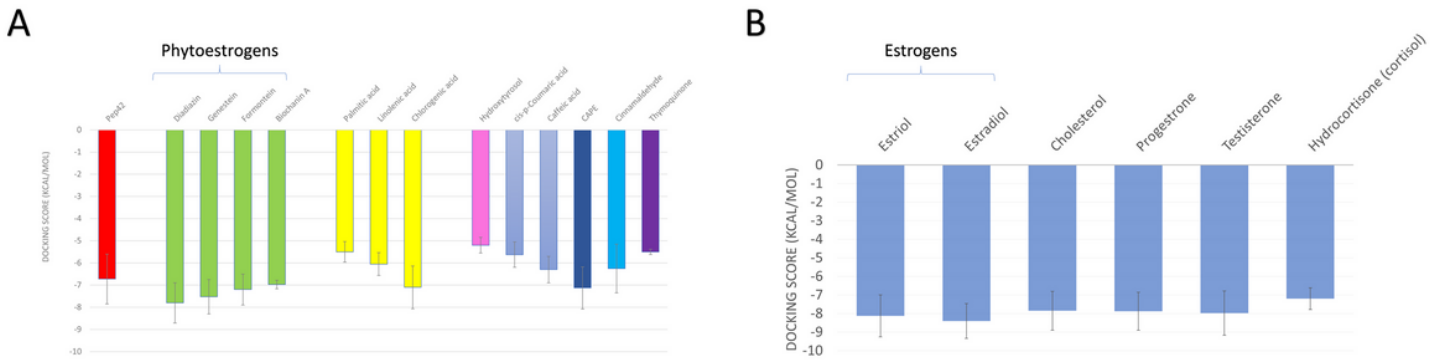

Figure 3

The average binding affinity (in kcal/mol) calculated using AutoDock Vina software for the docking of the natural products bioactive compounds (A) and physiological compounds (B) into the four different conformations of the HSPA5 SBDβ. The cyclic peptide Pep42 (red column) is used as a reference due to its specificity in binding HSPA5 in vivo. Estrogens and phytoestrogen are among the best binders to HSPA5 SBDβ.

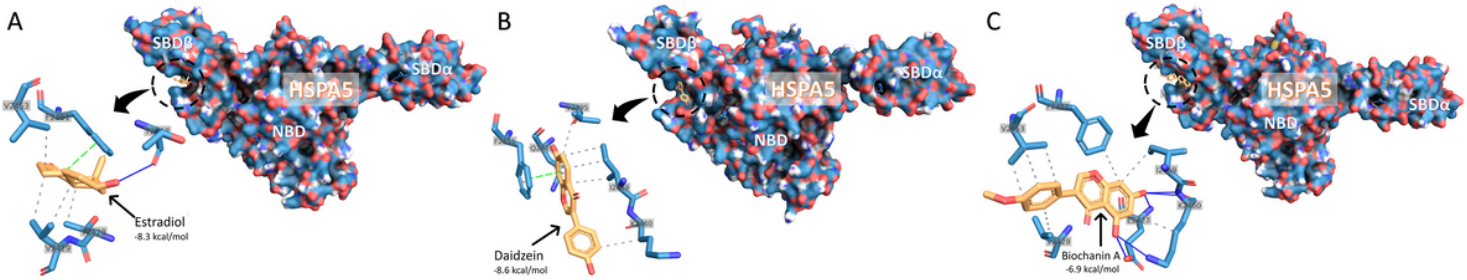

Figure 4

The structure of the docked complexes of HSPA5 and the small molecules (A) estradiol, (B) daidzein, and (C) biochanin A. HSPA5 is represented in the colored surface while the docked small molecules are in orange sticks. The NBD, SBDα, and SBDβ domains of the HSPA5 are labeled, while the enlarged panels show the interactions that established upon docking. The active site residues in the expanded panels are marked with its one-letter code and represented in blue sticks. H-bonds, hydrophobic contacts, and π-stacking interactions are shown by blue lines, dashed-gray lines, and dashed-green lines, respectively. The docking score (in kcal/mol) is shown for each complex.